Supplementary Methods

Cell Preparation and Labelling

To label actin filaments, HEK293 cells were grown to confluence on poly-L-lysine coated coverslips, fixed in 4% paraformaldehyde for 10 minutes and stained with Alexa488 conjugated Phalloidin (Molecular Probes A12379) according to the manufacturers protocol.

To image caveolin and ryanodine receptors (RyRs), ventricular myocytes were enzymatically isolated from an adult rat (6 weeks) according to the procedure described by Evans et al(1) and fixed in 2% paraformaldehyde for 10 minutes. They were then labelled according to a standard immunofluorescence protocol (2) using either a rabbit anti-caveolin primary (abcam ab2912-100) at a dilution of 500:1 and an Alexa 488 conjugated goat-anti-rabbit secondary (Molecular Probes A11034) at a dilution of 100:1, or a mouse-anti-RyR primary (Affinity BioReagents MA3-916) and an Alexa 488 conjugated goat-anti-mouse secondary (Molecular Probes A11029).

For imaging of actin labelling, coverslips with adherent HEK cells were inverted onto a 15 μL drop of PBS on a standard slide. To image ventricular myocytes, a 15 μL drop containing the myocytes suspended in PBS was sandwiched between a standard slide and a coverslip. The edges were then sealed with nail polish. Surface reflection interference imaging confirmed that the cells were in contact with the coverslip and thus suitable candidates for total internal reflection (TIRF) microscopy.

Microscope Hardware

Images were acquired on a commercial Nikon TE2000 inverted microscope with a Nikon TIRF2 TIRF adapter, a Nikon 60×, 1.49NA oil immersion TIRF objective, an Andor IXon DV887DCS-BV electron multiplying CCD camera, and a Laser Physics 150m Ar^+ laser providing $\sim 40\,mW$ on the $488\,nm$ line (which was selected by a line filter - MaxLine 488, Semrock). A fast shutter (Laser Physics - LST18) enabled computer control of the laser output. To increase the power density at the sample (to increase the depth of the

temporarily bleached state and reduce acquisition times) we replaced the Nikon stock fibre coupler at the microscope end with a coupler (F220FC-A, ThorLabs) producing a much narrower beam, corresponding to an illumination spot diameter of $\sim 2\ \mu m$ in the focal plane and a focal plane intensity of $\sim 200\ kW/cm^2$. Intensities were estimated from the entry power and measured efficiencies of the optical train without correcting for the boosted strength of the evanescent electric field.

An active correction of focus drift was performed by imaging the position of the imaging laser beam on a webcam after it had reflected from the coverslip and adjusting the position of the z-stage in a software feedback loop (similar to the scheme used by Huang et al(3)).

Image Acquisition

Images were acquired in TIRF mode using custom software and streamed to disk. An initial image was taken at a low ($\sim 1\ kW/cm^2$) illumination intensity and ($\sim 100\ ms$) integration time to minimise bleaching. For the subsequent reversible photo-bleaching series, an illumination intensity of $\sim 2 \times 10^5\ W/cm^2$, integration time of $14\ ms$, and an electorn multiplication gain setting of 150 (corresponding to an amplification of $\sim 80\times$) were selected. The integration time was chosen to match the typical on-time of single molecule events. Around 20000 frames were typically acquired to obtain images such as the ones shown, after which the number of localisation events per frame had typically dropped to less than $\sim 5\%$ of its starting value. The resulting per-image acquisition time was under 5 minutes.

Data Analysis

The choice of an integration time which matches the fluorophore on-time allowed us to analyse each frame independently with minimal loss of information. Single fluorophore events were detected as follows: A background image obtained by averaging the previous 10 frames was subtracted from the frame being analysed. This difference image was then filtered with a bandpass filter matched to the expected spot size, giving an image in which

only signals which had recently turned on are present.

To take account of the slightly variable illumination intensity across the field of view (due to the Gaussian beam profile of our illumination spot) a local thresholding procedure was applied to identify single molecule events. A local threshold was obtained by multiplying the local Poisson noise magnitude (estimated by taking the square root of the pixel values in the original image) with a scale factor approriate for the integration time and electron multiplication gain used.

Detected events were isolated from the threholded image using a standard labelling algorithm and the centre of intensity for each event was calculated. These point coordinates were starting parameters for a fitting procedure which uses the Levenburg-Marquardt algorithm(4, 5) to perform a weighted least squares fit of a Gaussian model function to the original unfiltered image data. The weights were chosen to reflect the Poisson noise characteristics of the CCD camera. The uneven bleaching of the sample allowed us to monitor x-y drift by using labelling at the edge of the field of view to measure, and potentially correct for, any drift. With care taken to keep room temperature constant and after any backlash in the x-y positioning stage had been given time to relax, this drift remained small over our acquisition time (< 5 min) and no correction was necessary for the images shown. The image analysis was conducted with custom written routines implemented in Python, using the freely available scientific library 'SciPy'(*www.scipy.org*). Performance critical segments (such as the Gaussian model function) were coded in C.

Image Reconstruction

The effective resolution in localisation microscopy depends on the number of molecules localised within a given area as well as molecule localisation accuracy, and may thus not be uniform throughout the image, but rather depends on the local labelling density. To reflect this fact, we have used a histogram technique with adaptive bin sizes to render localization images. The adaptive histogram is implemented as a quad-tree, with each localized event being assigned to a particular quadrant in the image. When the number of

localized molecules in a quadrant exceeds a pre-determined number (for the reconstructions shown this was chosen to be 3), the quadrant is itself quartered and the events redistributed amongst the new segments. This has the result that the number of events falling in each bin is approximately constant.

To produce an image where the intensity is proportional to the density of single molecule events, each of the leaf nodes of the quad-tree is rendered as a rectangle having an intensity equal to the number of events it contains divided by its area. The resulting image is blurred slightly (Gaussian, radius 1 pixel in reconstructed image/ 5 nm) to soften the sharp bin edges and remove any aliasing effects caused when bin and pixel boundaries do not perfectly coincide. The reconstructed images were then mildy saturated in ImageJ to allow weaker details to be seen.

Time resolved analysis of photo-bleaching

Cells were prepared as for imaging, and embedded in a mixture of glycerol and water. Antibody only samples were prepared by drying 10 μl droplets of Alexa488 labelled secondary (diluted in distilled water at a concentration of 1:400) onto clean glass coverslips. These were then mounted onto slides using various concentrations of glycerol in PBS as the embedding medium and the edges sealed with nail polish.

Images were taken in a small region of interest (to permit fast imaging), an integration time of $7\,ms$, and an electron multiplication gain setting of 150. The images were summed during acquisition to reduce data volume. The integrated intensity was recorded as the laser was switched on and off using a custom protocol whereby 10 s bleach intervals were interspersed with periods of darkness in which the fluorescence could recover. The length of these dark periods was ramped logarithmically from 5 s to a maximum of 1000 s, after which the ramp was reversed to obtain insight into the contribution of irreversible bleaching. Plotted traces were downsampled using a path simplification algorithm which preserved features larger than the linewidth.

References

1. Evans, A. M., and M. B. Cannell, 1997. The role of L-type Ca2+ current and Na+ current-stimulated Na/Ca exchange in triggering SR calcium release in guinea-pig cardiac ventricular myocytes. *Cardiovasc Res* 35:294–302.

2. Soeller, C., D. Crossman, R. Gilbert, and M. B. Cannell, 2007. Analysis of ryanodine receptor clusters in rat and human cardiac myocytes. *Proc Natl Acad Sci U S A* 104:14958–14963. `http://dx.doi.org/10.1073/pnas.0703016104`.

3. Huang, B., W. Wang, M. Bates, and X. Zhuang, 2008. Three-dimensional super-resolution imaging by stochastic optical reconstruction microscopy. *Science* 319:810–813. `http://dx.doi.org/10.1126/science.1153529`.

4. Levenberg, K., 1944. A method for the solution of certain problems in least squares. *Quart. Appl. Math* 2:164–168.

5. Marquardt, D., 1963. An Algorithm for Least-Squares Estimation of Nonlinear Parameters. *Journal of the Society for Industrial and Applied Mathematics* 11:431–441.

Figure S1: Reversible photobleaching in other organic dyes

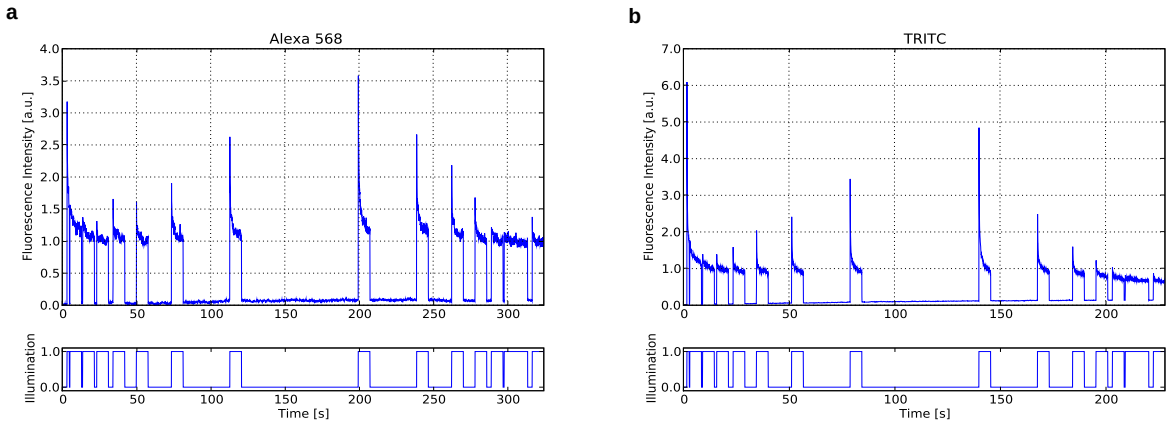

Reversible photobleaching in Alexa 568 (**a**) and TRITC (**b**) labelled secondary antibodies dried onto glass coverslips and illuminated at 532 nm. Note that this imaging was performed on dry samples, eliminating diffusion as a mechanism for fluorescence recovery. Similar results were observed with dried samples of Alexa 488 labelled secondary and unconjugated Fluorescein.

Figure S2: Solvent dependence of reversible photobleaching

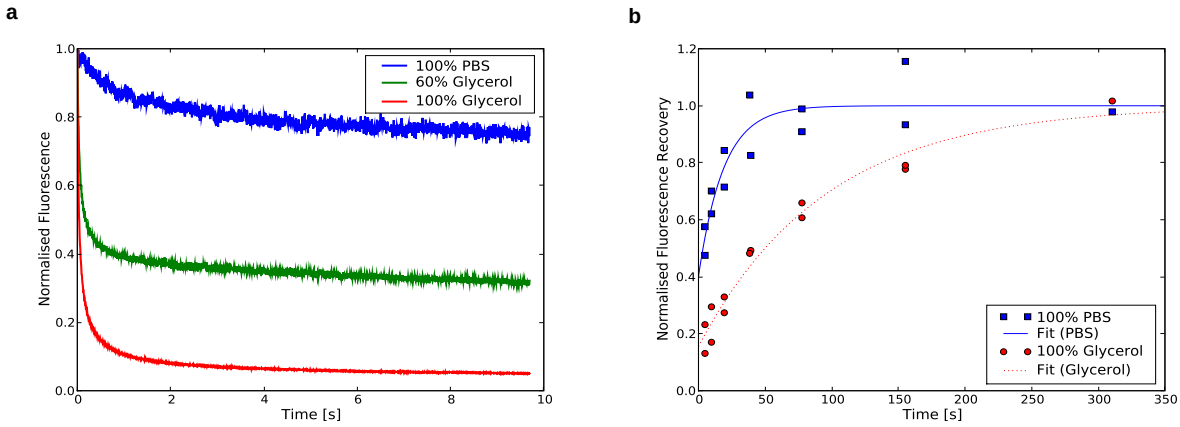

Dependence of the reversible photobleaching of Alexa 488 labelled antibodies on embedding media at a laser power of $\sim 25 kW/cm^2$. (**a**) - time course of bleaching in PBS, 60% glycerol in PBS, and glycerol. Intensity is dark-subtracted and normalised to the peak (pre-bleach) intensity in each case. The initial reversible bleaching is significantly faster in glycerol and the bleach-depth considerably deeper. (**b**) - solvent dependence of fluorescence recovery: fluorescence recovery was measured after various dark periods and fitted with a function of the form $I_r(t) = A(1 - be^{-t/\tau})$. The values were then normalised such that $I_r(\infty) = 1$ to enable the time courses to be compared (note that this obscures the fact the magnitude of the recovery was much larger in glycerol). The recovery is much faster in PBS which could also account for the lower bleaching depth in this solvent. Note that the lower laser power used for these measurements resulted in a reduced bleaching depth.

Figure S3: Intensity behaviour of single molecule events

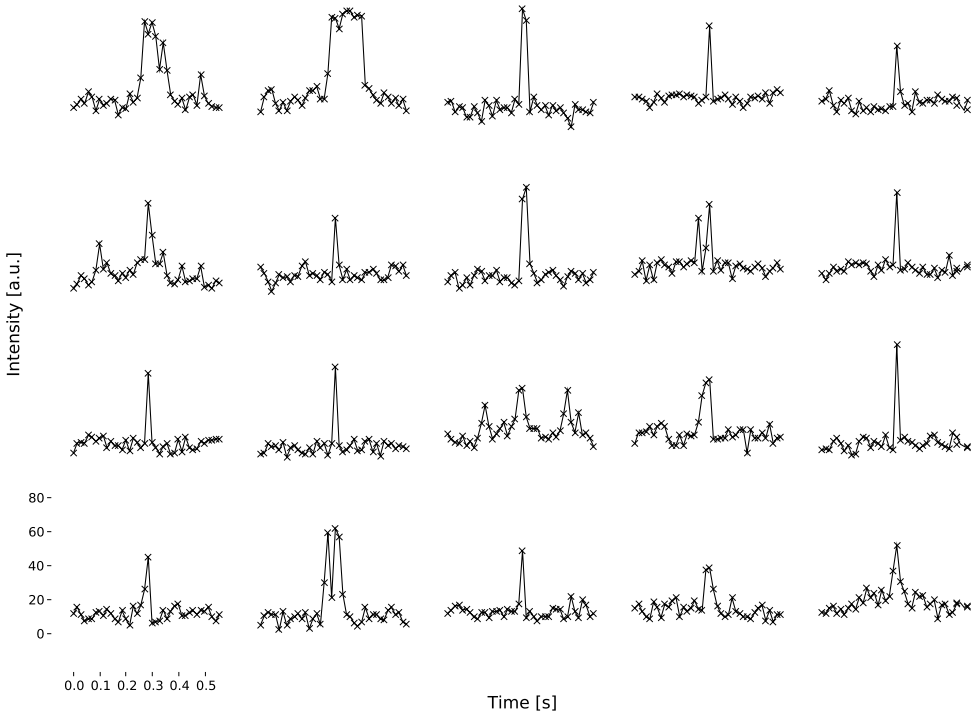

Intensity vs time profiles for 20 randomly selected events from the data set used to reconstruct the image in Fig 2b. The intensities were obtained by averaging over a 3x3 ROI centred at the location of the detected event. All profiles are consistent with single molecule events. Note that as our frame rate was chosen to match the average fluorophore on time, the edges of the discrete switching behaviour are not always well resolved. An on-off transition occurring in the middle of a frame will result in an intensity part way between the on and off intensities, and an apparent ramping up or down of fluorophore intensity.